# Dynamic Model of Hip and Ankle Joints Loading during Working with a Motorized Backpack Sprayer

**S. Karimi Avargani[1], A. Maleki2*, Sh. Besharati[3], R. Ebrahimi[4]**

1. M.Sc. Student of Mechanical Engineering of Biosystems Department, Faculty of Agriculture, Shahrekord University, Shahrekord, Iran
2. Associate Professor of Mechanical Engineering of Biosystems Department, Faculty of Agriculture, Shahrekord University, Shahrekord, Iran.
3. Lecture of Mechanical Engineering of Biosystems Department, Faculty of Agriculture, Shahrekord University, Shahrekord, Iran
4. Assistant Professor, Mechanical Engineering, Faculty of Engineering, Yasouj University, Yasouj, Iran

(Corresponding Author Email: maleki@sku.ac.ir)



## Abstract

The main objective of this paper is to develop a seven-link dynamic model for the operator's body while working with a motorized backpack sprayer. This model, includes the coordinates of the sprayer relative to the body, the rotational inertia of sprayer, the muscle moments acting on the joints and a kinematic coupling that keeps the body midway between the two legs. The constraint functions are determined and the non-linear differential equations of motion are derived using the Lagrange's equations. The results show that, undesirable fluctuations in the ankle force are noticeable at the beginning and end of the swing phase. Therefore, injuries to the ankle joint due to vibrations are more likely. The effects of engine speed and sprayer mass on the hip and ankle joint forces are then investigated. It is found that, the engine speed and sprayer mass have significant effects on the hip and ankle forces and can be used as effective control parameters. The results of the analysis also show that increasing the engine speed increases the frequency of the hip joint force; however, no significant effects on the frequency of the ankle joint force are observed. The results of this study may provide researchers with insight into estimating the allowable working hours with the motorized backpack sprayers, prosthesis design and load calculations of hip implants in the future.

**Keyword:** Lagrange equation; Operator; Vibration; Weight of sprayer.

**Symbols and abbreviations**

| Parameter | Description | Unite |
|---|---|---|
| $c_b$ | Distance from hip joint to center of mass (CoM) of upper body | *m* |
| $c_f$ | Distance from ankle joint to CoM of foot | *m* |
| $c_s$ | Distance from knee joint to CoM of shank | *m* |
| $c_t$ | Distance from hip joint to CoM of thigh | *m* |
| $e$ | Unbalance mass eccentricity | *mm* |
| $g$ | Gravitational acceleration | $ms^{-2}$ |
| $I_{sp}$ | Mass moments of inertia of sprayer about its principal axis | $kg.m^2$ |
| $l$ | Stance leg length | *m* |
| $l_s$ | Shank length | *m* |
| $l_t$ | Thigh length | *m* |
| $m_o$ | Unbalance mass of sprayer engine | *gr* |
| $m_b$ | Upper body mass | *kg* |
| $m_f$ | Foot mass | *kg* |
| $m_h$ | Hip mass | *kg* |
| $m_l$ | Leg mass | *kg* |
| $m_s$ | Shank mass | *kg* |
| $m_{sp}$ | Sprayer mass | *kg* |
| $m_t$ | Thigh mass | *kg* |
| $(x_{sp}, y_{sp})$ | Sprayer position from the CoM of upper body | *(m, m)* |
| $\omega$ | Engine speed | *rpm* |
| $x_h$ | Horizontal coordinate of hip joint | *M* |
| $y_h$ | Vertical coordinate of hip joint | *M* |
| $\theta_1$ | The angle between vertical axis and the stance leg | *Radian* |
| $\theta_2$ | The swing angle between vertical axis and the thigh | *Radian* |
| $\theta_3$ | The angle between vertical axis and the upper body | *Radian* |
| $\theta_{2s}$ | The swing angle between vertical axis and the shank | *Radian* |
| $\theta_{2f}$ | The angle between horizontal axis and foot | *Radian* |

## Introduction

One of the most popular ways of crop protection against weeds and pests is applying motorized backpack sprayers. Use of the motorized backpack sprayer eliminates the need for hand pumping, and it is suitable for small-scale farms. However, the major disadvantage of the motorized backpack sprayers is external forces acting on the operator's body (Kouchakzadeh, & Beigzadeh, 2015).

Forces acting in human body are important factors in the initiation and progression of joint disease (Astephen et al. 2008). Force analysis of hip and ankle joints can be useful in the development of strategies to avoid and manage conditions such as osteoarthritis and deterioration of femoroacetabular (Correa et al. 2010). Force analysis of hip and ankle joints requires multi-segment models.

Several research has been done on the dynamical modeling of the human body. Kuo (2001) applied a simple model of bipedal walking to evaluate simple hypotheses for metabolic cost of muscle activity. Tlalolini et al. (2010) optimized walking motions of a bipedal model by minimizing the value of the torque. The optimization process was carried out with and without the rotation of the supporting foot about the toe. Huang et al. (2012) employed a seven-link dynamic bipedal walking model with flat feet to analyze dynamics of walking. The results indicated that ankle stiffness plays different roles in different gaits. Martin and Schmiedeler (2014) proposed four and six link planar biped models with knees and rigid circular feet. The ankle was not considered in the four link model. The results showed that the model with ankles is more accurate in predicting energy consumption during normal human walking with different speeds. Sharbafi and Seyfarth (2015) utilized a five link model with a rigid upper body and two segmented legs to extract internal relations between joint's angles and stance leg orientation which hold the configuration harmonized during the gaits. Jena et al. (2016) developed a biomechanical model to predict metabolic energy consumption for carrying load manually by varying modes (head, shoulder and back), loads and ground inclinations. The results indicated that frontal torque (in shoulder mode) requires higher physiological energy than sagittal torque. Ma et al. (2022) presents the dynamic model of the human-prosthesis heterogeneous coupled system. Ma et al. (2023) also applied control strategies for prosthesis walking on stochastically uneven terrain.

Mechanical actions of the muscles are necessary for dynamical modelling of human's body and can be considered as moments applied at the joints. Weiss et al. (1986) indicated that the moment – angle relationships in the hip, knee and ankle joints are similar to a non-linear spring. Maletsky and Hillberry (2005) designed a dynamic knee simulator to reproduce the

loading and kinematics of the human knee during different activities. Lim and Park (2018) developed a model of human locomotion with curvy foot connected to leg by springy segment. so, the oscillations of the center of mass during walking can be described by the mechanics of a simple passive spring loaded inverted pendulum (SLIP). Kim et al. (2018) simulated joint reaction forces, active moments by muscles and passive moments by connective tissues. They found that, at the Chopart's and Lisfranc joints, passive moments were responsible for large portions of the net moments. The passive structures and passive moments in the midfoot joints provide strength to prevent injuries.

The need to carry backpack loads for long distances is common to a range of human endeavor. So, the influence of backpack carriage on physical performance has been investigated to establish guidelines for safe load limits. Liu (2007) analyzed the effect of backpack load position, walking speed and surface grade on the physiological responses of infantry soldiers. The results confirmed that locating the backpack mass center as near as possible to the body mass center results in the lowest energy consumption. Alamoudi et al. (2018) determined the effect of different carrying methods on walking stability using motion capture analysis. The results confirmed that lack of stability in frontal carriage forced the body to increase the cadence. Also, in order to minimize the moment generated by both the upper body and the heavy load, participants tended to decrease the length of their stride. Walsh et al. (2018) studied effect of stable and unstable load carriage on walking gait variability, dynamic stability and muscle activity of older adults. The results showed that unstable load carriage reduces dynamic stability compared to unloaded walking

Reviewing the literatures reveals that the investigation of the joint forces during load carrying is important for preventing the joint injuries. However, to date, no research has been published on the joint forces during the working with the motorized backpack sprayers. Therefore, the initial objective of the present study is to develop a seven-link dynamic model of operator's body during working with a motorized backpack sprayer. The secondary goal of this research is to examine the effects of different working conditions (engine speed and mass of sprayer) on the hip and ankle joint forces. This is a continuation of our previous work, where the torque – angle relationships in the hip, knee and ankle joints for the backpack sprayer operator body were discussed (Karimi et al. 2020).

**Material and methods**

In this section, the principle of the Lagrange equation for nonholonomic constraints are introduced. The total kinetic energy, potential energy, generalized forces and constraints are

expressed for the proposed model. The non-linear equations of motion are formulated by the Lagrange's equations and solved using Maple.

**Lagrange Equation for Nonholonomic Constraints**

Lagrange's equations occupy a special place in analytical mechanics. They represent equations of motion in terms of generalized coordinates. A holonomic constrain in the system of $n$ generalized coordinates $q_i$ can be written in the following form:

$$g_j(q_1, q_2, ..., q_n, t) = 0 \quad (1)$$

For the nonholonomic constraints, equation (1) changes to the followed differential form (D'Souza & Garg (1984); Greenwood (1988)):

$$\sum_{\upsilon=1}^{n} a_{l\upsilon} dq_\upsilon + a_{lt} dt = 0 \qquad l=1, 2, \ldots, s \quad (2)$$

where $\upsilon=1, 2, \ldots, n$ and $l=1, 2, \ldots, s$ are number of coordinates and number of constraints, respectively ($n>s$). The Lagrange's equation for constrained systems is expressed as

$$\frac{d}{dt}\left(\frac{\partial T}{\partial \dot{q}_\upsilon}\right) - \frac{\partial T}{\partial q_\upsilon} + \frac{\partial V}{\partial q_\upsilon} - \sum_{l=1}^{s} \lambda_l a_{l\upsilon} = Q_\upsilon \qquad \upsilon = 1, 2, \ldots, n \quad (3)$$

where $T$, $V$, $\lambda_l$, and $Q_v$ are kinetic energy, potential energy, Lagrange's coefficients and generalized force related to generalized coordinate $q_i$, respectively. These $n$ equations involve $n+s$ unknown quantities, namely the $n$ coordinates $q_v$ and the $s$ Lagrange multipliers $\lambda_l$. the additionally needed equations are just the s constraint equations (2) which couple the $q_v$; however, these are now to be considered as differential equations:

$$\sum_{\upsilon=1}^{n} a_{l\upsilon} \dot{q}_\upsilon + a_{lt} = 0 \qquad l=1, 2, \ldots, s \quad (4)$$

**Dynamic model of operator's body during spraying**

Figure 1 shows the proposed dynamical model of operator's body during working with a motorized backpack sprayer. This model includes two rigid legs interconnected individually through a hinge with a rigid upper body connected at the hip. Each leg includes thigh, shank, and foot. The thigh and the shank are connected at the knee joint. The foot and the shank are connected at the ankle joint. A point mass $m_h$ at hip represents the pelvis. The mass of upper body $m_b$, leg $m_l$, thigh $m_t$, shank $m_s$ and foot $m_f$ are considered as lumped parameters. Longitudinal parameters $c_b$, $c_f$, $c_l$, $c_s$, $c_t$, $l$, $l_s$ and $l_t$ are distance from hip joint to Center of Mass (CoM) of upper body, distance from ankle joint to CoM of foot, distance from hip joint to CoM of stance leg, distance from knee joint to CoM of shank, distance from hip joint to

CoM of thigh, stance leg length, shank length, and thigh length, respectively. The motorized backpack sprayer is located at position ($x_{sp}$, $y_{sp}$) from the CoM of upper body.

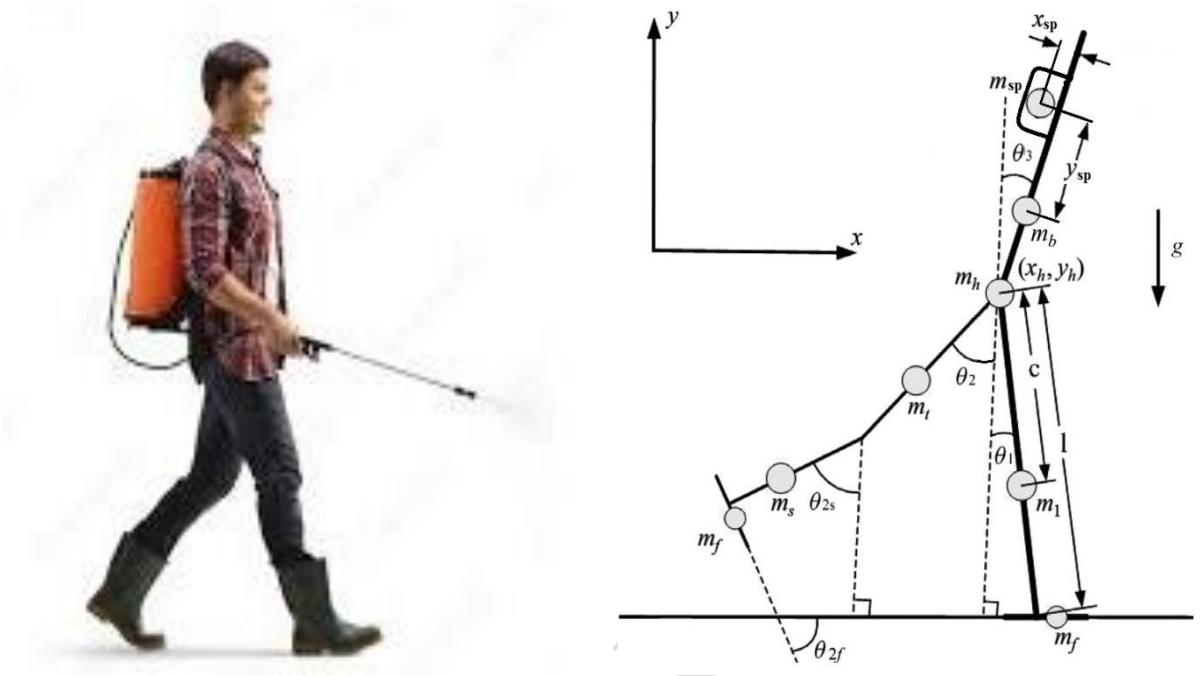


**Fig. 1.** The proposed dynamical model of operator's body during working with a motorized backpack sprayer

The total kinetic energy, potential energy, generalized forces and constraints are expressed using the following assumptions (Wisse et al. 2004):

- The joints have no damping or friction.
- Bones suffering no flexible deformation
- A kinematic coupling has been used in the model to keep the body midway between the two legs.
- The shank of the stance foot is always locked and the whole leg can be modeled as one rigid stick.
- The friction between the walker and the ground is enough. Thus, the flat feet do not deform or slip.
- The muscle moments acting on the hip, knee and ankle joints are modeled as non-linear torsional springs.
- The sprayer engine consists of unbalance force. This can be due to deposition or erosion of rotational parts material.

**Kinetic Energy**

As shown in Fig. 1, it is assumed that the *x*-axis is along the ground while the *y*-axis is vertical to the ground upward. Dynamical model of operator's body during working with a motorized backpack sprayer can be described by the following generalized coordinates:

$$\underset{\sim}{q}^T = [x_h, y_h, \theta_1, \theta_2, \theta_3, \theta_{2s}, \theta_{2f}] \tag{5}$$

where $x_h$, $y_h$, $\theta_1$, $\theta_2$, $\theta_3$, $\theta_{2s}$ and $\theta_{2f}$ are horizontal coordinate of hip joint, vertical coordinate of hip joint, the angle between vertical axis and the stance leg, the swing angle between vertical axis and the thigh, the angle between vertical axis and the upper body, the swing angle between vertical axis and the shank and the angle between horizontal axis and foot, respectively. The positive directions of all the angles are counterclockwise. The total kinetic energy of the system is defined as the sum of the kinetic energy of the point masses, translational and rotational kinetic energy of the motorized backpack sprayer. So, the obtained expression for the kinetic energy is given as follow:

$$\begin{aligned}
T &= T_h + T_l + T_t + T_b + T_{sp} + T_s + T_f \qquad (6)\\
&= \frac{1}{2}[m_h + m_l + m_t + m_b + m_{sp} + m_s + m_f]\dot{x}_h^2 \\
&\quad + \frac{1}{2}[m_h + m_l + m_t + m_b + m_{sp} + m_s + m_f]\dot{y}_h^2 \\
&\quad + \frac{1}{2}m_l c_l^2 \dot{\theta}_1^2 + \frac{1}{2}\left[m_t c_t^2 + m_s l_t^2 + m_f l_t^2\right]\dot{\theta}_2^2 \\
&\quad + \frac{1}{2}\left[I_{sp} + m_b c_b^2 + m_{sp}\left[\left(c_b + y_{sp}\right)^2 + x_{sp}^2\right]\right]\dot{\theta}_3^2 \\
&\quad + \frac{1}{2}\left[m_s c_s^2 + m_f l_s^2\right]\dot{\theta}_{2s}^2 + \frac{1}{2}m_f c_f^2 \dot{\theta}_{2f}^2 + m_l c_l \dot{\theta}_1\left(\dot{x}_h \cos\theta_1 + \dot{y}_h \sin\theta_1\right) \\
&\quad - m_t c_t \dot{\theta}_2\left(\dot{x}_h \cos\theta_2 - \dot{y}_h \sin\theta_2\right) + m_b c_b \dot{\theta}_3\left(\dot{x}_h \cos\theta_3 - \dot{y}_h \sin\theta_3\right) \\
&\quad + m_{sp}\dot{\theta}_3\left\{\left[\left(c_b + y_{sp}\right)\dot{x}_h + x_{sp}\dot{y}_h\right]\cos\theta_3 + \left[x_{sp}\dot{x}_h - \left(c_b + y_{sp}\right)\dot{y}_h\right]\sin\theta_3\right\} \\
&\quad + m_s\left\{l_t c_s \dot{\theta}_2 \dot{\theta}_{2s}\cos\left(\theta_2 - \theta_{2s}\right) - \dot{x}_h\left[l_t\dot{\theta}_2\cos\theta_2 + c_s\dot{\theta}_{2s}\cos\theta_{2s}\right] + \dot{y}_h\left[l_t\dot{\theta}_2\sin\theta_2 + c_s\dot{\theta}_{2s}\sin\theta_{2s}\right]\right\} \\
&\quad + m_f\left\{l_s l_t \dot{\theta}_2 \dot{\theta}_{2s}\cos\left(\theta_2 - \theta_{2s}\right) + c_f l_t \dot{\theta}_2 \dot{\theta}_{2f}\sin\left(\theta_{2f} - \theta_2\right) + c_f l_s \dot{\theta}_{2s}\dot{\theta}_{2f}\sin\left(\theta_{2f} - \theta_{2s}\right)\right. \\
&\qquad - \dot{x}_h\left[l_t\dot{\theta}_2\cos\theta_2 + l_s\dot{\theta}_{2s}\cos\theta_{2s} + c_f\dot{\theta}_{2f}\sin\theta_{2f}\right] \\
&\qquad \left. + \dot{y}_h\left[l_t\dot{\theta}_2\sin\theta_2 + l_s\dot{\theta}_{2s}\sin\theta_{2s} - c_f\dot{\theta}_{2f}\cos\theta_{2f}\right]\right\}
\end{aligned}$$

where $I_{sp}$, is mass moments of inertia of sprayer about its principal axis, respectively.

**Potential Energy**

The total potential energy of the system is defined as the sum of the gravitational energy of the point masses. So, the general expression for the potential energy is

$$\begin{aligned} U &= U_h + U_l + U_t + U_b + U_{sp} + U_s + U_f \\ &= -\left[ m_h l + m_l (l - c_l) + m_t l + m_b l + m_{sp} l + m_s l \right] g (1 - \cos\theta_1) \\ &\quad + \left[ m_t c_t + m_s l_t \right] g (1 - \cos\theta_2) - \left[ m_b c_b + m_{sp} (c_b + y_{sp}) \right] g (1 - \cos\theta_3) \\ &\quad + m_{sp} g x_{sp} \sin\theta_3 + m_s g c_s (1 - \cos\theta_{2s}) \\ &\quad + m_f g (l \cos\theta_1 - l_t \cos\theta_2 - l_s \cos\theta_{2s} - c_f \sin\theta_{2f}) \end{aligned} \tag{7}$$

**Generalized Forces**

The generalized forces acting on the operator's body during working with a motorized backpack sprayer include forces resulting from gravity, unbalance due to erosion of sprayer engine, muscle moment acting on the hip joint, muscle moment acting on the knee joint and muscle moment acting on the ankle joint. The generalized forces $Q_{qi}$ are given by the following equations:

$$Q_{x_h} = m_0 e \omega^2 \cos(\omega t) \tag{8}$$

$$Q_{y_h} = m_0 e \omega^2 \sin(\omega t) \tag{9}$$

$$Q_{\theta_1} = T_{1f} \tag{10}$$

$$Q_{\theta_2} = T_2 \tag{11}$$

$$\begin{aligned} Q_{\theta_3} &= m_0 e \omega^2 \cos\omega t [(c_b + y_{sp}) \cos\theta_3 + x_{sp} \sin\theta_3] \\ &\quad + m_0 e \omega^2 \sin\omega t [-(c_b + y_{sp}) \sin\theta_3 + x_{sp} \cos\theta_3] \end{aligned} \tag{12}$$

$$Q_{\theta_{2s}} = T_{2s} \tag{13}$$

$$Q_{\theta_{2f}} = 0 \tag{14}$$

where $m_0$, $e$ and $\omega$ are unbalance mass of sprayer engine, unbalance mass eccentricity and engine speed, respectively.

The muscle moment acting on the hip joint $T_2$ (the swing leg), muscle moment acting on the knee joint $T_{2s}$ (the swing leg) and muscle moment acting on the ankle joint $T_{1f}$ (stance leg) are non-linear functions of angle between the two segments (Karimi et al. 2020).

$$T_2 = 0.0007(\theta_2 - \theta_3)^3 - 0.0258(\theta_2 - \theta_3)^2 + 0.3236(\theta_2 - \theta_3) - 1.6792 \tag{15}$$

$$T_{2s} = -0.0011(\theta_{2s} - \theta_2)^2 - 0.0029(\theta_{2s} - \theta_2) + 1.2683 \tag{16}$$

$$T_{1f} = 0.0043\theta_1^3 + 0.0429\theta_1^2 + 0.5052\theta_1 + 3.1455 \tag{17}$$

**Constraints**

A constraint can be expressed by some relationship between generalized coordinates and time. When foot contact of the stance leg with ground is maintained, first and second constraint equations can be represented as

$$y_h - l\cos\theta_1 = 0 \tag{18}$$

$$x_h + l\sin\theta_1 - x_{ankle} = 0 \tag{19}$$

where $x_{ankle}$ is the fixed position of the ankle of the stance leg. In the passive dynamical model of human walking, the upper body can be considered as an inverted pendulum jointed around the hip. So, a kinematic coupling has been used in the model to keep the upper body between the two legs and achieve a stable walking (Wisse et al. 2004). The equation of the kinematic coupling constraint is introduced according to:

$$2\theta_3 - (\theta_1 + \theta_2) = 0 \tag{20}$$

Time course of hip, knee and ankle joint angles for the proposed model are given as follows (Karimi et al. 2020):

$$\theta_2 - \theta_3 = 373.64t^3 - 762.66t^2 + 414.86t - 38.89 \tag{21}$$

$$\theta_{2s} - \theta_2 = -6357.5t^3 + 4911.3t^2 - 958.48t + 1.24 \tag{22}$$

$$\theta_1 = 451.84t^3 - 513.31t^2 + 218.5t - 27.77 \tag{23}$$

According to equation (4), the constraint equations (18) - (23) can be considered in differential form:

$$\dot{y}_h + l\sin\theta_1\dot{\theta}_1 = 0 \tag{24}$$

$$\dot{x}_h + l\cos\theta_1\dot{\theta}_1 = 0 \tag{25}$$

$$\dot{\theta}_1 + \dot{\theta}_2 - 2\dot{\theta}_3 = 0 \tag{26}$$

$$\dot{\theta}_2 - \dot{\theta}_3 - 1120.92t^2 + 1525.32t - 414.86 = 0 \tag{27}$$

$$\dot{\theta}_2 - \dot{\theta}_{2s} - 19072.5t^2 + 9822.6t - 958.48 = 0 \tag{28}$$

$$\dot{\theta}_1 - 1355.52t^2 + 1026.62t - 218.5 = 0 \tag{29}$$

By applying the Lagrange's equation (3) and introducing the constant coefficients, seven coupled non-linear differential equations of motion can be obtained as

$$\eta_1\ddot{x}_h+\eta_2\cos\theta_1\ddot{\theta}_1-\eta_3\cos\theta_2\ddot{\theta}_2+\left[\eta_4\cos\theta_3+\eta_5\sin\theta_3\right]\ddot{\theta}_3-\eta_6\cos\theta_{2s}\ddot{\theta}_{2s} \quad (30)$$
$$-\eta_7\sin\theta_{2f}\ddot{\theta}_{2f}-\eta_2\sin\theta_1\dot{\theta}_1^2+\eta_3\sin\theta_2\dot{\theta}_2^2-\left[\eta_4\sin\theta_3-\eta_5\cos\theta_3\right]\dot{\theta}_3^2$$
$$+\eta_6\sin\theta_{2s}\dot{\theta}_{2s}^2-\eta_7\cos\theta_{2f}\dot{\theta}_{2f}^2+\lambda_2=m_0e\omega^2\cos(\omega t)$$

$$\eta_1\ddot{y}_h+\eta_2\sin\theta_1\ddot{\theta}_1+\eta_3\sin\theta_2\ddot{\theta}_2-\left[\eta_4\sin\theta_3-\eta_5\cos\theta_3\right]\ddot{\theta}_3+\eta_6\sin\theta_{2s}\ddot{\theta}_{2s} \quad (31)$$
$$-\eta_7\cos\theta_{2f}\ddot{\theta}_{2f}+\eta_2\cos\theta_1\dot{\theta}_1^2+\eta_3\cos\theta_2\dot{\theta}_2^2-\left[\eta_4\cos\theta_3+\eta_5\sin\theta_3\right]\dot{\theta}_3^2$$
$$+\eta_6\cos\theta_{2s}\dot{\theta}_{2s}^2+\eta_7\sin\theta_{2f}\dot{\theta}_{2f}^2+\lambda_1=m_0e\omega^2\sin(\omega t)$$

$$\eta_8\ddot{\theta}_1+\eta_2\left(\cos\theta_1\ddot{x}_h+\sin\theta_1\ddot{y}_h\right)-\eta_9 g\sin\theta_1+\lambda_1 l\sin\theta_1+\lambda_2 l\cos\theta_1+\lambda_3+\lambda_6 \quad (32)$$
$$=0.0043\theta_1^3+0.0429\theta_1^2+0.5052\theta_1+3.1455$$

$$\eta_{10}\ddot{\theta}_2-\eta_3\cos\theta_2\ddot{x}_h+\eta_3\sin\theta_2\ddot{y}_h+\eta_{11}\cos\left(\theta_2-\theta_{2s}\right)\ddot{\theta}_{2s}+\eta_{12}\sin\left(\theta_{2f}-\theta_2\right)\ddot{\theta}_{2f} \quad (33)$$
$$+\eta_{11}\sin\left(\theta_2-\theta_{2s}\right)\dot{\theta}_{2s}^2+\eta_{12}\cos\left(\theta_{2f}-\theta_2\right)\dot{\theta}_{2f}^2+\eta_3 g\sin\theta_2+\lambda_3+\lambda_4+\lambda_5$$
$$=0.0007(\theta_2-\theta_3)^3-0.0258(\theta_2-\theta_3)^2+0.3236(\theta_2-\theta_3)-1.6792$$

$$\eta_{13}\ddot{\theta}_3+(\eta_4\cos\theta_3+\eta_5\sin\theta_3)\ddot{x}_h-(\eta_4\sin\theta_3-\eta_5\cos\theta_3)\ddot{y}_h-\eta_4 g\sin\theta_3 \quad (34)$$
$$+\eta_5 g\cos\theta_3-2\lambda_3-\lambda_4=m_0e\omega^2\cos\omega t\left[(c_b+y_{sp})\cos\theta_3+x_{sp}\sin\theta_3\right]$$
$$-m_0e\omega^2\sin\omega t\left[(c_b+y_{sp})\sin\theta_3-x_{sp}\cos\theta_3\right]$$

$$\eta_{14}\ddot{\theta}_{2s}-\eta_6\cos\theta_{2s}\ddot{x}_h+\eta_6\sin\theta_{2s}\ddot{y}_h+\eta_{11}\cos\left(\theta_2-\theta_{2s}\right)\ddot{\theta}_2+\eta_{15}\sin\left(\theta_{2f}-\theta_{2s}\right)\ddot{\theta}_{2f} \quad (35)$$
$$-\eta_{11}\sin\left(\theta_2-\theta_{2s}\right)\dot{\theta}_2^2+\eta_{15}\dot{\theta}_{2f}^2\cos\left(\theta_{2f}-\theta_{2s}\right)+\eta_6 g\sin\theta_{2s}-\lambda_5=$$
$$=-0.0011(\theta_{2s}-\theta_2)^2-0.0029(\theta_{2s}-\theta_2)+1.2683$$

$$c_f\ddot{\theta}_{2f}-\sin\theta_{2f}\ddot{x}_h-\cos\theta_{2f}\ddot{y}_h+l_t\sin\left(\theta_{2f}-\theta_2\right)\ddot{\theta}_2+l_s\sin\left(\theta_{2f}-\theta_{2s}\right)\ddot{\theta}_{2s} \quad (36)$$
$$-l_t\cos\left(\theta_{2f}-\theta_2\right)\dot{\theta}_2^2-l_s\cos\left(\theta_{2f}-\theta_{2s}\right)\dot{\theta}_{2s}^2-g\cos\theta_{2f}=0$$

The constant coefficients $\eta_i$ (i=1, 2, … ,15) are defined in the Appendix. In order to analyze dynamical behavior of the operator's body during working with a motorized backpack sprayer, it is necessary to solve thirteen coupled non-linear differential equations (24) - (36) for $x_h$, $y_h$, $\theta_1$, $\theta_2$, $\theta_3$, $\theta_{2s}$, $\theta_{2f}$, $\lambda_1$, $\lambda_2$, $\lambda_3$, $\lambda_4$, $\lambda_5$ and $\lambda_6$.

**Hip and ankle joints forces in the swing phase**

Forces in human joints are important factors in the initiation and progression of joint disease. Investigation of the joint forces have made it possible to prevent or minimize discomfort, fatigue or risk of injuries. In this section, the hip and ankle joint forces in the model of operator's body during working with a motorized backpack sprayer are calculated. Considering the upper body, Newton's second law leads to the following equations:

$$\sum F_x = m_b \ddot{x}_{m_b} + m_{sp} \ddot{x}_{m_{sp}} + m_0 e\omega^2 \cos(\omega t) \tag{37}$$

$$\sum F_y = m_b \ddot{y}_{m_b} + m_{sp} \ddot{y}_{m_{sp}} + m_0 e\omega^2 \sin(\omega t) \tag{38}$$

The components of the hip joint force become

$$F_{x_h} = m_b(\ddot{x}_h + c_b \cos\theta_3 \ddot{\theta}_3) + m_{sp}(\ddot{x}_h + x_{sp} \sin\theta_3 \ddot{\theta}_3 + (c_b + y_{sp}) \cos\theta_3 \ddot{\theta}_3) + m_0 e\omega^2 \cos(\omega t) \tag{39}$$

$$F_{y_h} = m_b(\ddot{y}_h - c_b \sin\theta_3 \ddot{\theta}_3) + m_{sp}(\ddot{y}_h + x_{sp} \cos\theta_3 \ddot{\theta}_3 - (c_b + y_{sp}) \sin\theta_3 \ddot{\theta}_3) + m_0 e\omega^2 \sin(\omega t) + (m_{sp} + m_b) g \tag{40}$$

Finally, the total hip joint force is

$$F_h = \sqrt{F_{x_h}^2 + F_{y_h}^2} \tag{41}$$

Considering the full body, Newton's second law leads to the following equation:

$$\sum F_x = m_b \ddot{x}_{m_b} + m_f \ddot{x}_{m_f} + m_h \ddot{x}_{m_h} + m_l \ddot{x}_{m_l} + m_s \ddot{x}_{m_s} + m_{sp} \ddot{x}_{m_{sp}} + m_t \ddot{x}_{m_t} + m_0 e\omega^2 \cos(\omega t) \tag{42}$$

The x-directional force of the hip joint become

$$\begin{aligned} F_{x_f} = {} & m_b(\ddot{x}_h + c_b \cos\theta_3 \ddot{\theta}_3) + m_f(\ddot{x}_h - l_s \cos\theta_{2s} \ddot{\theta}_{2s} - l_t \cos\theta_2 \ddot{\theta}_2 - c_f \sin\theta_{2f} \ddot{\theta}_{2f}) \\ & + m_h \ddot{x}_h + m_l(l - c_l) \cos\theta_1 \ddot{\theta}_1 + m_s(\ddot{x}_h - c_s \cos\theta_{2s} \ddot{\theta}_{2s} - l_t \cos\theta_2 \ddot{\theta}_2) \\ & + m_{sp}(\ddot{x}_h + x_{sp} \sin\theta_3 \ddot{\theta}_3 + (c_b + y_{sp}) \cos\theta_3 \ddot{\theta}_3) \\ & + m_t(\ddot{x}_h - c_t \cos\theta_2 \ddot{\theta}_2) + m_0 e\omega^2 \cos(\omega t) \end{aligned} \tag{43}$$

Considering the stance leg, the calculation of moment about the hip joint leads to the following equation:

$$F_{y_f} = m_l c_l (l - c_l) \ddot{\theta}_1 + m_l g c_l \sin\theta_1 - F_{x_f} l \cos\theta_1 \big/ l \sin\theta_1 \tag{44}$$

Finally, the total ankle joint force is

$$F_f = \sqrt{F_{x_f}^2 + F_{y_f}^2} \tag{45}$$

**Results and discussion**

The values of physical parameters related to the analysis are listed in Table 1. Thirteen coupled non-linear differential equations (24) - (36) are solved in Maple. Fig. 2 illustrates the effects of engine speed and mass of sprayer on the hip and ankle joint forces during working with a motorized backpack sprayer.

It can be observed that the ankle force is fluctuating in the beginning of the swing phase (*t=[0.1-0.2]*). It stays nearly constant at *t=[0.2-0.4]*. Again, fluctuations of the ankle force appear in the end of the swing phase (*t=[0.4-0.5]*). The first fluctuation range is because of

the ‘toe-off’. At the instant of the ‘toe-off’, the toe loses contact with ground. The second fluctuation range is because of the ‘heel-strike’. At the instant of the ‘heel-strike’, there is an impact between the swing leg and the ground when the heel of the swing leg contacts the ground. The maximum force can exert on the joints when the operator begins to swing forward (‘toe-off’). Also, at the instants of the ‘toe-off’ and ‘heel-strike’ undesirable variations of ankle joint force $F_h$ are noticeable. So, ankle injuries due to vibration exposure are more likely.

From a comparison between the Fig. 2(a) and (b) it reveals that the frequency of the hip joint force increases with increasing the engine speed $\omega$. However, considerable effects on frequency of the ankle joint force have not been observed. Also, with increasing the engine speed $\omega$, amplitudes of both the hip and ankle joint force increases.

**Table 1.** The values of physical parameters (Huang et al. (2012))

| Parameter | Value |
|---|---|
| Distance from hip joint to CoM of upper body, $c_b$ | *0.262 m* |
| Distance from ankle joint to CoM of foot, $c_f$ | *0.017 m* |
| Distance from knee joint to CoM of shank, $c_s$ | *0.157 m* |
| Distance from hip joint to CoM of thigh, $c_t$ | *0.192* |
| Unbalance mass eccentricity, $e$ | *5 mm* |
| Gravitational acceleration, $g$ | *9.81 m/s$^2$* |
| Mass moments of inertia of sprayer about its principal axis, $I_{sp}$ | *Kg.m$^2$* |
| Stance leg length, $l$ | *0.700 m* |
| Shank length, $l_s$ | *0.315 m* |
| Thigh length, $l_t$ | *0.385 m* |
| Unbalance mass of sprayer engine, $m_o$ | *0.01 gr* |
| Upper body mass, $m_b$ | *26.62 Kg* |
| Foot mass, $m_f$ | *2.66 Kg* |
| Hip mass, $m_h$ | *19.97 Kg* |
| Leg mass, $m_l$ | *11.53 Kg* |
| Shank mass, $m_s$ | *3.45 Kg* |
| Sprayer mass, $m_{sp}$ | *10.50 Kg* |
| Thigh mass, $m_t$ | *8.07 Kg* |
| Sprayer position from the CoM of upper body, ($x_{sp}$, $y_{sp}$) | *(0.175m, 0.038m)* |
| Engine speed, $\omega$ | *3000 rpm* |

From a comparison between the Fig. 2(a) and (c) it reveals that increasing the mass of sprayer $m_{sp}$ leads to small reduction in oscillation of ankle joint force. Also, with increasing the mass of sprayer $m_{sp}$, magnitude of both the hip and ankle joint forces increases.

Fig. 3 exhibits the effect of leg length on the hip and ankle joint forces during working with a motorized backpack sprayer. It can be observed that the frequency of the hip joint force increases with decreasing the leg length *l*. This is because the stance leg keeps contact with ground while the swing leg pivots about the constraint hip like pendulum. So, shorter operators are more vulnerable to injuries due to vibration exposure.

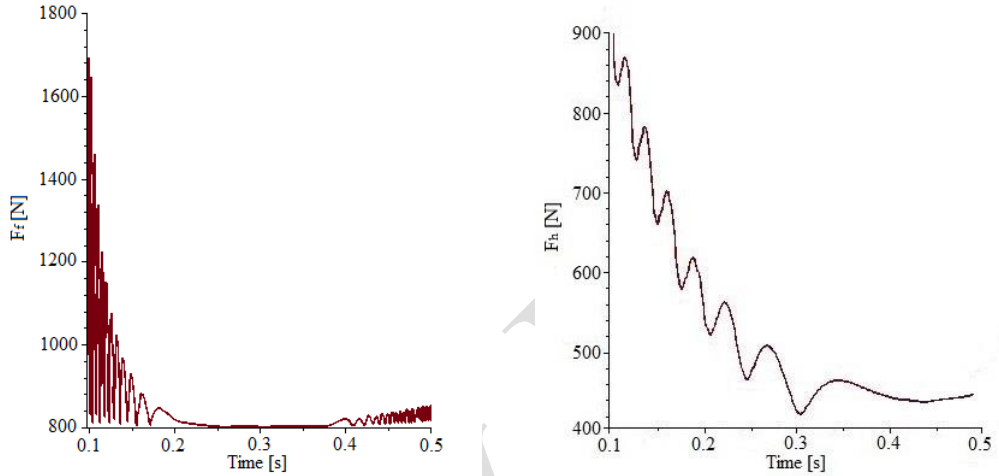


*a) ω=3000 rpm, $m_{sp}$=10.5 kg, l=0.7 m*

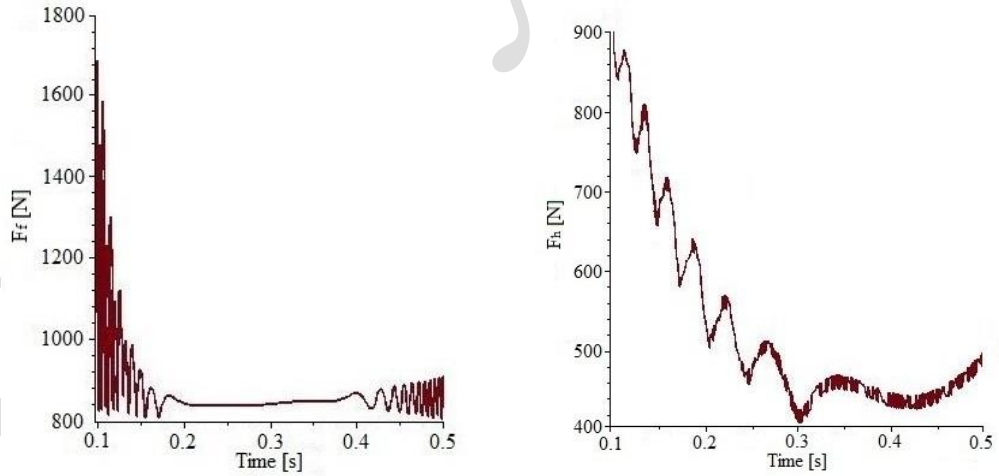


*b) ω=6000 rpm, $m_{sp}$=10.5 kg, l=0.7 m*

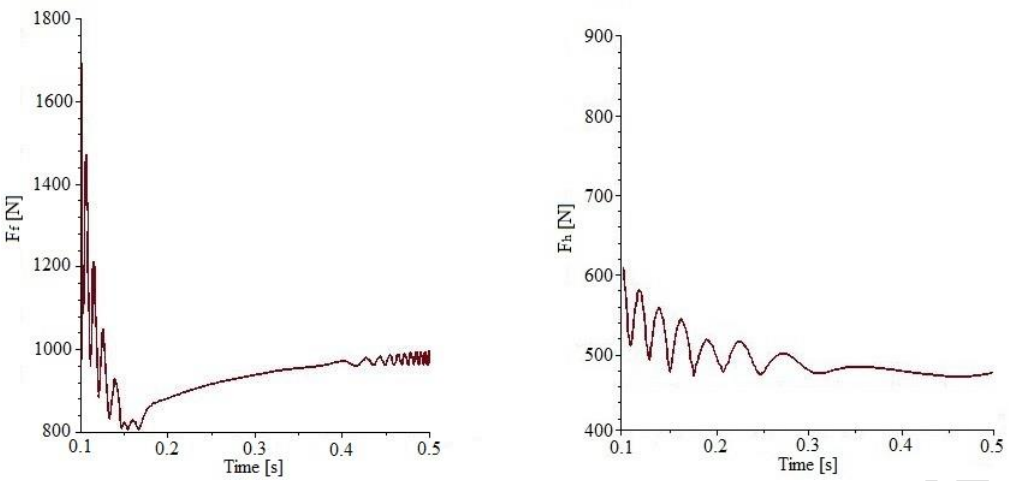


*c) ω=3000 rpm, $m_{sp}$=12.5 kg, l=0.7 m*

**Fig. 2.** The hip joint force $F_h$ and ankle joint force $F_f$ for (a) $m_{sp}$=10.5 kg, ω=3000 rpm, l=0.7 m (b) $m_{sp}$=10.5 kg, ω=6000 rpm , l=0.7 m (c) $m_{sp}$=12.5 kg, ω=3000 rpm, l=0.7 m.

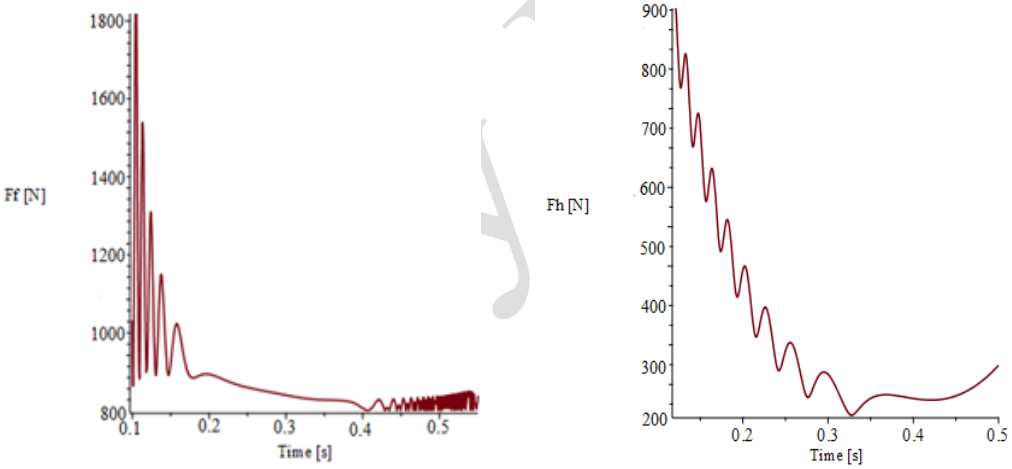


*a) ω=3000 rpm, $m_{sp}$=10.5 kg, l=0.88 m*

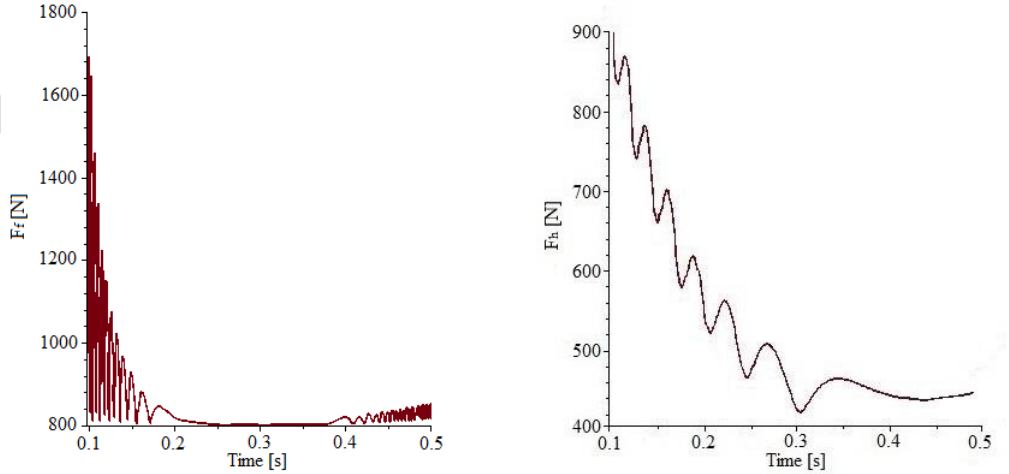

*b) ω=3000 rpm, $m_{sp}$=10.5 kg, l=0.7 m*

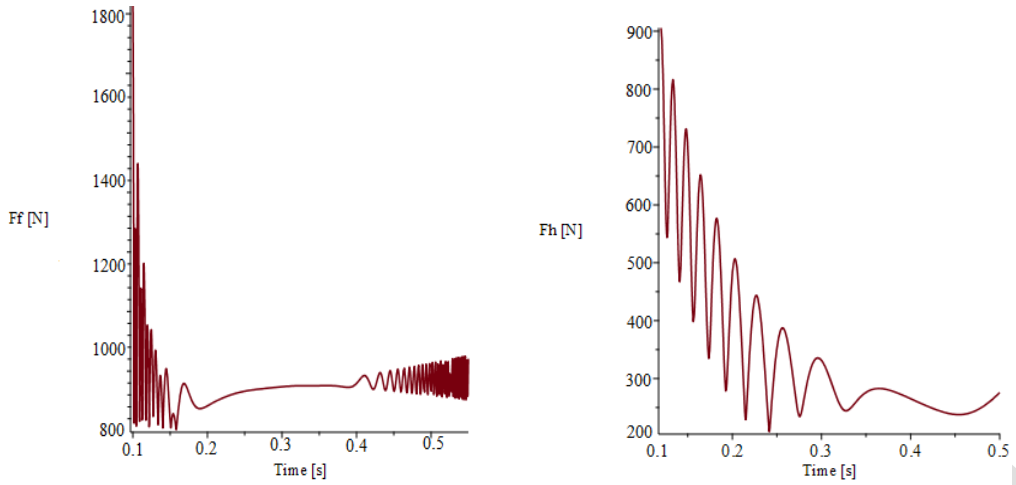


*c) ω=3000 rpm, $m_{sp}$=10.5 kg, l=0.6 m*

**Fig. 3.** The hip joint force $F_h$ and ankle joint force $F_f$ for (a) *$m_{sp}$=10.5 kg, ω=3000 rpm, l=0.7 m* (b) *$m_{sp}$=10.5 kg, ω=6000 rpm , l=0.7 m* (c) *$m_{sp}$=12.5 kg, ω=3000 rpm, l=0.7 m.*

## Conclusion

In this study, a novel assistive dynamical model for the operator's body during working with a motorized backpack sprayer was presented. In this model, the coordinate of the sprayer relative to the body, rotational inertia of sprayer, muscle moments acting on joints and a kinematic coupling confining the upper body between the two legs, were considered. Dynamics of sprayer operator was described by seven generalized coordinates. The non-linear equations of motion were obtained using the Lagrange's equations. The results obtained from the numerical analysis indicated that, in the beginning and end of the swing phase, ankle injuries due to vibration exposure are more probable. Moreover, the maximum force can exert on the joints in early swing phase. Also, the effects of engine speed and mass of sprayer on the hip and ankle joint forces were studied. It is found that the larger mass of sprayer (full capacity of tank), can lead to higher level of joint forces and lower oscillations. The frequency of hip and ankle joint forces increased with the increase of the engine speed. The results of this paper can be used for estimation of patient condition and implant design. Investigation the effects of anthropometric specifications and sprayer position (relative to the body) on the hip and ankle joint forces during working with a motorized backpack sprayer are important topic to study in the future.

**Key Points:**

- Development of a seven-link dynamic model of operator's body during working with a motorized backpack sprayer
- The non-linear differential equations of motion are formulated by the Lagrange's equations and solved in Maple
- Study the effects of engine speed and mass of sprayer on the hip and ankle joint forces

## Appendix

The constant coefficients of Eqs. (30) – (36) are as follows:

$$\eta_1 = m_h + m_l + m_t + m_b + m_{sp} + m_s + m_f \qquad \eta_2 = m_l c_l$$

$$\eta_3 = m_t c_t + m_s l_t + m_f l_t \qquad \eta_4 = m_b c_b + m_{sp}\left(c_b + y_{sp}\right)$$

$$\eta_5 = m_{sp} x_{sp} \qquad \eta_6 = m_s c_s + m_f l_s$$

$$\eta_7 = m_f c_f \qquad \eta_8 = m_l c_l^2$$

$$\eta_9 = \eta_1 l - m_l c_l \qquad \eta_{10} = m_t c_t^2 + m_s l_t^2 + m_f l_t^2$$

$$\eta_{11} = l_t \eta_6 \qquad \eta_{12} = m_f l_t c_f$$

$$\eta_{13} = I_{sp} + m_b c_b^2 + m_{sp}\left[\left(c_b + y_{sp}\right)^2 + x_{sp}^2\right] \qquad \eta_{14} = m_s c_s^2 + m_f l_s^2$$

$$\eta_{15} = m_f l_s c_f$$

**Acknowledgements:** The authors would like to thank the University of Shahrekord for providing the laboratory facilities and financial support for this research

## References

Alamoudi, M., Travascio, F., Onar-Thomas, A., Eltoukhy, M., & Asfour, S. (2018). The effects of different carrying methods on locomotion stability, gait spatio-temporal parameters and spinal stresses. *International Journal of Industrial Ergonomics, 67,* 81-88. https://doi.org/10.1016/j.ergon.2018.04.012

Astephen, J. L., Deluzio, K. J., Caldwell, G. E., & Dunbar, M. J. (2008). Biomechanical changes at the hip, knee, and ankle joints during gait are associated with knee osteoarthritis severity. *Journal of orthopaedic research*, *26*(3), 332-341. https://doi.org/10.1002/jor.20496

Correa, T. A., Crossley, K. M., Kim, H. J., & Pandy, M. G. (2010). Contributions of individual muscles to hip joint contact force in normal walking. *Journal of biomechanics*, *43*(8), 1618-1622. https://doi.org/10.1016/j.jbiomech.2010.02.008

D'Souza, A. F., & Garg, V. K. (1984). *Advanced dynamics: modeling and analysis*. Prentice Hall.

Greenwood, D. T. (1988). *Principles of dynamics* (pp. 224-226). Englewood Cliffs, NJ: Prentice-Hall.

Huang, Y., Wang, Q., Chen, B., Xie, G., & Wang, L. (2012). Modeling and gait selection of passivity-based seven-link bipeds with dynamic series of walking phases. *Robotica*, *30*(1), 39-51. https://doi.org/10.1017/S0263574711000397

Jena, S., Kumar, A., Singh, J. K., & Mani, I. (2016). Biomechanical model for energy consumption in manual load carrying on Indian farms. *International Journal of Industrial Ergonomics*, *55*, 69-76. https://doi.org/10.1017/S0263574711000397

Karimi Avargani, S., Maleki, A., Besharati, S., & Ebrahimi, R. (2020). Muscle moment and angle of hip, knee and ankle joints in a seven-link model of backpack sprayer operator. *Iranian Journal of Ergonomics*, *8*(3), 36-47. http://dx.doi.org/10.30699/jergon.8.3.36

Kim, Y., Lee, K. M., & Koo, S. (2018). Joint moments and contact forces in the foot during walking. *Journal of biomechanics*, *74*, 79-85. https://doi.org/10.1016/j.jbiomech.2018.04.022

Kouchakzadeh, A., & Beigzadeh, Y. (2015). Permitted working hours with a motorised backpack sprayer. *biosystems engineering*, *136*, 1-7. https://doi.org/10.1016/j.biosystemseng.2015.05.005

Kuo, A. D. (2001). A simple model of bipedal walking predicts the preferred speed–step length relationship. *J. Biomech. Eng.*, *123*(3), 264-269. https://doi.org/10.1115/1.1372322

Lim, H., & Park, S. (2018). Kinematics of lower limbs during walking are emulated by springy walking model with a compliantly connected, off-centered curvy foot. *Journal of biomechanics*, *71*, 119-126. https://doi.org/10.1016/j.jbiomech.2018.01.031

Liu, B. S. (2007). Backpack load positioning and walking surface slope effects on physiological responses in infantry soldiers. *International Journal of Industrial Ergonomics*, *37*(9-10), 754-760. https://doi.org/10.1016/j.ergon.2007.06.001

Ma, X., Xu, J., Fang, H., Lv, Y., & Zhang, X. (2022). Adaptive Neural Control for Gait Coordination of a Lower Limb Prosthesis. *International Journal of Mechanical Sciences*, 215, 106942. https://doi.org/10.1016/j.ijmecsci.2021.106942

Ma, X., Xu, J., & Zhang, X. (2023). Bilateral constrained control for prosthesis walking on stochastically uneven terrain. *International Journal of Mechanical Sciences*, 239, 107896. https://doi.org/10.1016/j.ijmecsci.2022.107896

Maletsky, L. P., Hillberry, B. M. (2005). Simulating dynamic activities using a five-axis knee simulator. *Journal of Biomechanical Engineering*, 127, 123-133. https://doi.org/10.1115/1.1846070

Martin, A. E., & Schmiedeler, J. P. (2014). Predicting human walking gaits with a simple planar model. *Journal of biomechanics*, *47*(6), 1416-1421. https://doi.org/10.1016/j.jbiomech.2014.01.035

Sharbafi, M. A., & Seyfarth, A. (2015, May). Mimicking human walking with 5-link model using HZD controller. In *2015 IEEE International Conference on Robotics and Automation (ICRA)* (pp. 6313-6319). IEEE. https://doi.org/10.1109/ICRA.2015.7140086

Tlalolini, D., Chevallereau, C., & Aoustin, Y. (2010). Human-like walking: Optimal motion of a bipedal robot with toe-rotation motion. *IEEE/ASME Transactions on Mechatronics*, *16*(2), 310-320. https://doi.org/10.1109/TMECH.2010.2042458

Walsh, G. S., Low, D. C., & Arkesteijn, M. (2018) Effect of stable and unstable load carriage on walking gait variability, dynamic stability and muscle activity of older adults. *Journal of Biomechanics*, 73, 18-23. https://doi.org/10.1016/j.jbiomech.2018.03.018

Weiss, P. L., Kearney, R. E., & Hunter, I. W. (1986). Position dependence of ankle joint dynamics—I. Passive mechanics. *Journal of biomechanics*, *19*(9), 727-735. https://doi.org/10.1016/0021-9290(86)90196-X

Wisse, M., Schwab, A. L., & van der Helm, F. C. (2004). Passive dynamic walking model with upper body. *Robotica*, *22*(6), 681-688. https://doi.org/10.1017/S0263574704000475

# مدل‌سازی دینامیکی بار وارد بر مفاصل ران و مچ پا ، هنگام کار با سمپاش پشتی موتوری

صدیقه کریمی آورگانی [۱]، علی ملکی [۲*]، شاهین بشارتی [۳]، رضا ابراهیمی [۴]

۱. دانشجوی کارشناسی ارشد گروه مهندسی مکانیک بیوسیستم، دانشکده کشاورزی، دانشگاه شهرکرد، شهرکرد ایران
۲. دانشیار و عضو هیات علمی گروه مهندسی مکانیک بیوسیستم، دانشکده کشاورزی، دانشگاه شهرکرد، شهرکرد، ایران.
۳. مربی گروه مهندسی مکانیک بیوسیستم، دانشکده کشاورزی، دانشگاه شهرکرد، شهرکرد، ایران
۴. استادیار، گروه مهندسی مکانیک، دانشکده فنی و مهندسی، دانشگاه یاسوج، یاسوج، ایران

(نویسنده مسئول: maleki@sku.ac.ir)

هدف اصلی این مقاله توسعه یک مدل دینامیک هفت لینکی از بدن اپراتور در هنگام کار با سمپاش کوله پشتی موتوری است. این مدل شامل مختصات سمپاش نسبت به بدن، اینرسی چرخشی سمپاش، گشتاور ماهیچه‌ای وارد بر روی مفاصل و یک کوپلینگ سینماتیک که در بین دو پا نگه برای حفظ تعادل بدن در نظر گرفته شده است. محدودیت توابع تعیین شدند و معادلات دیفرانسیل غیر خطی حرکت توسط معادلات لاگرانژ استخراج شدند. نتایج نشان می دهد که در ابتدا و انتهای مرحله نوسان، تغییرات نامطلوب نیروی مفصل مچ پا قابل توجه است. بنابراین، آسیب مچ پا به دلیل قرار گرفتن در معرض ارتعاش احتمال بیشتری دارد. سپس اثرات سرعت چرخش موتور و جرم سمپاش بر نیروهای مفصل ران و مچ پا بررسی شد. سرعت چرخش موتور و جرم سمپاش اثرات قابل توجهی بر نیروهای مفصل ران و مچ پا دارد و می تواند به عنوان پارامترهای کنترلی موثر مورد استفاده قرار گیرد. همچنین، نتایج آنالیز نشان می‌دهد که با افزایش سرعت چرخش موتور، فرکانس نیروی مفصل ران افزایش می‌یابد. با این حال، اثرات قابل توجهی بر فرکانس نیروی مفصل مچ پا مشاهده نشده است. نتایج به دست امده از این تحقیق می‌تواند برخی از بینش‌ها را به محققان در براورد ساعات کار مجاز با سمپاش های کوله پشتی موتوری، طراحی پروتز و محاسبات استرس ایمپلنت های لگن و در آینده ارائه دهد.